RESEARCH ARTICLE

Blends of Bio-Based Poly(Limonene Carbonate) with Commodity Polymers

Simon Neumann, Pin Hu, Felix Bretschneider, Holger Schmalz, and Andreas Greiner*

In this study, blends of the bio-based poly(limonene carbonate) (PLimC) with different commodity polymers are investigated in order to explore the potential of PLimC toward generating more sustainable polymer materials by reducing the amount of petro- or food-based polymers. PLimC is employed as minority component in the blends. Next to the morphology and thermal properties of the blends the impact of PLimC on the mechanical properties of the matrix polymers is studied. The interplay of incompatibility and zero-shear melt viscosity contrast determines the blend morphology, leading for all blends to a dispersed droplet morphology for PLimC. Blends with polymers of similar structure to PLimC (i.e., aliphatic/aromatic polyester) show the best performance with respect to mechanical properties, whereas blends with polystyrene or poly(methyl methacrylate) are too brittle and polyamide 12 blends show very low elongations at break. In blends with Ecoflex (poly(butylene adipate-co-terephthalate)) and Arnitel EM400 (copoly(ether ester)) with poly(butylene terephthalate) hard and polytetrahydrofuran soft segments) a threefold increase in E-modulus can be achieved, while keeping the elongation at break at reasonable high values of ≈200%, making these blends highly interesting for applications.

1. Introduction

Based on the limitation of fossil resources, the development of bio-based and sustainable polymers and their corresponding blends is a highly relevant and intensively studied field of research.[1] Several bio-based synthetic polymers are made from naturally derived monomers and show biodegradability, like poly(hydroxy alkanoates) (PHA), poly(butylene succinate) (PBS), or poly(*L*-lactic acid) (PLA).[2] CO_2 is one of the interesting candidates as a sustainable C1 building block for polymers, because it is non-toxic, cheap, and highly available. It can react with epoxides via alternating ring-opening copolymerization (ROCOP) to polycarbonates.[3,4] Limonene oxide (LO) is next to menth-2-ene oxide (Men2C) one of the few bio-based epoxides and can be directly produced by oxidizing naturally occurring limonene (main component from citrus oil) to yield bio-based polycarbonates via ROCOP with CO_2.[5,6] About 57 000 t a^{-1}[7] of citrus oil are gathered as side product from the orange juice production, representing a non-food based feedstock for LO[4] which is insufficient for the industrial production of polymers. This feedstock could be extended further by full exploitation of the orange crop worldwide. Meanwhile, any chemical use of limonene as raw material of the chemical industry will require microbial production of the terpene from truly abundant bio-based raw materials such as sugars. Synthesis of poly(limonene carbonate) (PLimC) by ROCOP of *trans*-LO and CO_2 was first introduced by Coates et al.,[8] employing a β-diiminate zinc complex ([(bdi)Zn(μ-OAc)]. Further on, in 2015 Kleij et. al. developed an Al(III) aminotriphenolate complex for the synthesis of PLimC.[9,10] In the last 5 years, lot of research efforts have been focused on PLimC.[9–11] The synthesis of high molar mass PLimC (M_n ≈100 kg mol^{-1}) by using [(bdi)Zn(μ-OAc)] as catalyst was achieved by masking hydroxyl impurities in *trans*-LO, as demonstrated by Hauenstein et al.[6] This high molar mass PLimC features a high glass transition temperature ($T_g = 130\,°C$), high transparency (99.8%), high light transmission (95%) and Young´s modulus ($E = 0.95$ GPa). PLimC has also a high gas permeability for oxygen and CO_2, which can be made use of in "breathing glass" applications.[12] A highly versatile and efficient route for PLimC modification is based on thiol-ene click chemistry, which allows to tailor properties like solubility, T_g or subsequent cross-linking for coating applications.[13] Moreover, the living character of ROCOP catalyzed by [(bdi)Zn(μ-OAc)] allows the synthesis of well-defined PLimC-*block*-poly(cyclohexene carbonate) diblock copolymers, showing an interesting phase behavior with a rather broad stability range for the HPL (hexagonal perforated lamella) morphology.[14] The market potential of PLimC has been recently assessed by Parrino et al.[15] and Zhang et al.[16] They show that PLimC can be an useful non-toxic, bio-based alternative for bisphenol A based polycarbonates, which use highly toxic monomers, such as phosgene and bisphenol A. According to Zhang et al., PLimC is a potential replacement for fossil based polystyrene (PS), because the

S. Neumann, Dr. P. Hu, F. Bretschneider, Dr. H. Schmalz, Prof. A. Greiner
Macromolecular Chemistry and Bavarian Polymer Institute
University of Bayreuth
Universitätsstraße 30, 95440 Bayreuth, Germany
E-mail: greiner@uni-bayreuth.de

**ADVANCED
SCIENCE NEWS**

www.advancedsciencenews.com

**Macromolecular
Materials and Engineering**

www.mame-journal.de

Table 1. Characteristics of the employed polymers and processing conditions for blend preparation.

Polymer	Grade	Supplier	$M_n/Đ$ [a]	δ [b]	η_0 [c]	Processing temperature
			[kDa] /–	[MPa$^{1/2}$]	[kPa s]	[°C]
PLimC	–	–	65/1.1	17.6[14]	890[25]	–
PLA	Inego 4060D	Nature Works	64/1.7	20.7[26]	4.2[27]	190
PBAT	Ecoflex, BASF F Blend A1200	BASF SE	45/1.3	22.3[28]	2.7[29]	180
COPE	Arnitel EM400	DSM	75/1.5	19.2[30]	0.275[31]	200
PA12	Vestamid Typ L1600	Evonik Industries	40/1.4	20.8[30]	0.390[32]	185
PMMA	PLEXIGLAS 8N	Evonik Industries	57/1.6	18.6[33]	0.071[34]	180
PS	BASF 143E	BASF SE	121/2.0	18.7[33]	–	180

[a] Number average molecular weight (M_n) and dispersity (Đ) were determined by CHCl$_3$-GPC and HFIP-GPC, calibrated with narrowly distributed PS (CHCl$_3$-GPC) and PMMA (HFIP-GPC) standards; [b] Solubility parameter; [c] Zero-shear melt viscosity.

production costs of both polymers are quite similar ($\approx$\$1.36–\$1.51 kg^{-1}).[16] An easy and cost-efficient method to produce materials with new properties is blending. The currently technically used bio-based polymers, such as PLA, are mainly used in the form of blends (e.g., in blends with polyglycols,[17] poly(vinyl acetate),[18] polypropylene,[19] or styrene resins[20]). Also blends of degradable poly(butylene adipate-*co*-terephthalate) ((poly(butylene adipate-co-terephthalate)) (PBAT), Ecoflex) and PLA with improved mechanical properties were established.[21] The importance of PHA[22] and PBS[23] blends as well as bio-based blends in general have been highlighted in several publications and reviews.[24] One advantage of employing PLimC in blends, next to its sustainability, is its high glass transition temperature (T_g = 130 °C), which can lead to blends with increased heat resistance. Besides, due to its high glass transition temperature neat PLimC is usually rather brittle and exhibits a comparably low elongation at break. Together with the high melt viscosity of PLimC, which is inherently attributed to its stiff polymer backbone, melt processing of neat PLimC usually requires the use of additives like bio-based ethyl oleate.[25] Hence, the use of bio-based PLimC as minority component in polymer blends represents an elegant method to harness its high glass transition temperature without encountering difficulties in melt processing due to its high melt viscosity and the need to use additional additives.

In this contribution PLimC blends (10–30 wt% PLimC) with engineering or commodity plastics have been explored with the aim to gain an basic understanding of PLimC blends which could lead to future sustainable polymer materials. As matrix polymers for blending with PLimC we considered polymers with similar structure, like aliphatic/aromatic polyesters and polyamides, to ensure a good combability (i.e., PLA, PBAT, polyamide 12 (PA12), (copoly(ether ester)) (COPE). Additionally, commodity plastics with similar glass transition temperatures (poly(methyl methacrylate) (PMMA) or PS) were also employed. The different blend systems were investigated with respect to their morphology, thermal, and mechanical properties. The outcome of the basic understanding of the present PLimC blends with selected commodity polymers should be the starting point for future developments for tuning of blends properties toward more sustainable und useful polymer materials.

2. Results and Discussion

2.1. Selection and Specifications of Blend Components

PLA, PA12, PBAT (Ecoflex), and a COPE (Arnitel EM400) were selected as matrix polymers for PLimC blends because of their similar chemical structure (polyesters, polyamides) to PLimC. PS (T_g = 100 °C) and PMMA (T_g = 117 °C) were chosen as polymers with glass transition temperatures close to that of PLimC (T_g = 130 °C). Compatibility of the used polymers with PLimC can be estimated by comparing the polymer solubility parameters (δ). As the solubility parameters are significantly different from PLimC (**Table 1**), phase separation is expected for all blend systems. Melt viscosity and molecular weight of the investigated polymers are also playing a significant role in the blending process, because PLimC has by far the highest zero-shear melt viscosity (Table 1). Consequently, at the employed weight fractions (10–30 wt%) PLimC is expected to form the dispersed phase in the blend and the matrix will be formed by the polymer with the lower melt viscosity. Characteristics of the employed polymers and processing parameters for blending are summarized in Table 1.

Blends with PS and PMMA were found to be inhomogeneous and/or very brittle and, thus, were not pursued further. An overview of these blend systems and their mechanical data can be found in the supporting information (Figure S1 and Table S1, Supporting Information). In the following, the morphology and thermal/mechanical properties of the other blend systems will be discussed starting with PLA (aliphatic polyester), followed by PBAT (aromatic/aliphatic polyester), Arnitel EM400 (segmented aromatic COPE) and PA12 (aliphatic polyamide).

2.2. Blends with PLA

The effect of blending PLA with bio-based PLimC is addressed in the following. PLA/PLimC blends are opaque in comparison to neat PLA, which is transparent (Figure S2, Supporting Information), indicating phase separation in PLA/PLimC blends. Morphology investigation with scanning electron microscopy (SEM) reveals a homogenous dispersion of spherical PLimC droplets in the PLA matrix for blends with 10 and 30 wt% PLimC, respectively (**Figure 1**). PLimC is forming the dispersed phase, because it is the minority component and the melt viscosity of PLimC

**ADVANCED
SCIENCE NEWS**

www.advancedsciencenews.com

**Macromolecular
Materials and Engineering**

www.mame-journal.de
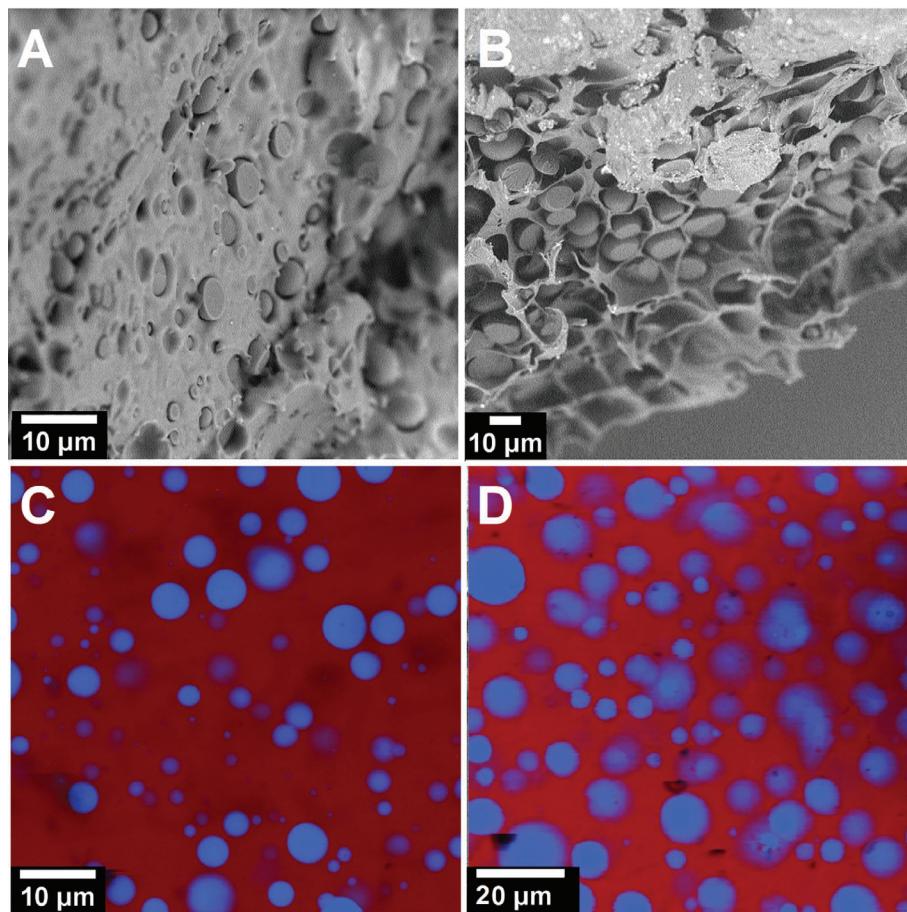
Figure 1. SEM and Raman imaging of PLA/PLimC blends: A,C) PLA/PLimC = 90/10 w/w; B,D) PLA/PLimC = 70/30 w/w. In (C) and (D) the domains colored in blue represent PLimC droplets that are embedded in the PLA matrix (colored in red). The Raman spectra of each component are given in Figure S4, Supporting Information.

(η_0 = 890 kPa··s)[25] is significantly higher compared to that of PLA (η_0 = 4.2 kPa·s)[27] (Table 1). As a result, the shear forces during melt processing are not sufficient to deform or split the PLimC droplets further. From SEM measurements, an average PLimC droplet diameter of D = 3.6 ± 3.9 μm (PLA/PLimC = 90/10 w/w) and D = 6.0 ± 6.1 μm (PLA/PLimC = 70/30 w/w) from surface fractures can be extracted (**Table 2** and Figure S3, Supporting Information). For the calculation of the droplet size, the area of each PLimC droplet was measured using the ImageJ software.[35] Then, assuming that droplets are fully spherical particles and the fracture have gone through the middle of each droplet, the diameter corresponding to the area was back calculated. Of course, these assumptions cannot be 100% fulfilled, hence resulting in the relatively high standard deviations. PLimC and PLA can be nicely distinguished based on their Raman spectra (Figure S4, Supporting Information), which enables the use of Raman imaging for morphological studies. Comparing SEM with Raman imaging shows values for the PLimC droplet diameters in the same order of magnitude (PLA/PLimC = 90/10 w/w: D = 2.8 ± 3.0 μm, PLA/PLimC = 70/30 w/w: D = 7.1 ± 7.2 μm). The corresponding domain size distributions are presented in the Supporting Information (Figure S5 and Table S2, Supporting Information).

Thermal properties of PLA/PLimC blends (Table 2 and **Figure 2**) were investigated by differential scanning calorimetry (DSC) and thermogravimetric analysis (TGA). Comparing the glass transition temperatures (T_g) of PLA in PLA/PLimC blend systems with neat PLA shows similar values at ≈60 °C, as it would be expected from a phase-separated blend. The T_g of PLimC (T_g = 128 °C, Figure S6, Supporting Information) could not be recognized, because T_g is superimposed with the cold crystallization of PLA at T_{cc} ≈ 120 °C (Figure 2A) and the PLimC fraction is very low, so the sensitivity limit of the DSC is reached.

Interestingly, PLA/PLimC blends show cold crystallization (T_{cc} ≈ 120 °C) and melting (T_m ≈ 170 °C) in the second heating runs (Table 2 and Figure 2A), whereas pure PLA displays these characteristics only in the first heating trace (not shown). In the corresponding cooling traces a weak exothermic peak at T_c ≈ 100 °C can be detected (Figure 2B), which can be attributed to a partial crystallization of PLA and is also in the same range where cold crystallization (T_{cc} ≈ 120 °C) was observed in the second heating traces. This might point to a nucleation effect of the PLimC droplets on PLA crystallization, an effect that has also been observed for the matrix of the other blend systems studied (see discussion in following sections). Strong nucleation effects were also found by Rizzuto et al., who investigated

Table 2. PLimC droplet sizes and thermal/mechanical properties of the produced blends.

	PLimC droplet sizes[a] SEM/Raman imaging		Thermal[b]					Mechanical[c]		
	Domain area [µm²]	Equivalent diameter [µm]	T_g [°C]	T_{cc} [°C]	T_m [°C]	T_c [°C]	$T_{5\%}$ [°C]	σ_m [MPa]	ϵ_{br} [%]	E-modulus [MPa]
PLimC (neat)	–	–	130	–	–	–	230	42 ± 0.37	15 ± 4	972 ± 95
PLA blends										
PLA (neat)	–	–	61	–	–	–	335	58 ± 3	2.7 ± 0.2	3520 ± 112
10 wt% PLimC	10.3 ± 6/6.2 ± 13	3.6 ± 3.9/2.8 ± 3.0	60	116	170	–	n.d.	57 ± 0.3	2.1 ± 0.1	3454 ± 22
30 wt% PLimC	28 ± 24/40 ± 14	6.0 ± 6.1/7.1 ± 7.3	61	117	172	100	250/335	36 ± 1	1.39 ± 0.1	3050 ± 56
PBAT blends										
PBAT (neat)	–	–	–30	–	122	42	370	36 ± 3.0	1376 ± 103	92 ± 19
10 wt% PLimC	1.9 ± 2.4/1.4 ± 1.0	1.6 ± 1.7/1.3 ± 1.9	–28	–	128	84	n.d.	17 ± 1.2	659 ± 43	99 ± 3.0
30 wt% PLimC	1.0 ± 0.7/0.6 ± 0.5	1.1 ± 1.8/0.90 ± 1.8	–28	–	131	89	253/370	10 ± 0.19	184 ± 50	247 ± 12
COPE blends										
COPE (neat)	–	–	–72	–	0.9/197	–30/122	377	25 ± 1.5	1013 ± 111	34.3 ± 5.8
10 wt% PLimC	0.1 ± 0.1/0.3 ± 0.2	0.4 ± 1.3/0.6 ± 1.8	–70	–	4.9/200	–28/173	n.d.	21 ± 0.70	930 ± 76	49.7 ± 5.4
30 wt% PLimC	1.9 ± 3.8/0.49 ± 0.25	1.5 ± 1.7/0.8 ± 1.9	–70	–	5.5/199	–30/178	250/377	14 ± 1.2	193 ± 44	146 ± 11
PA12 blends										
PA12 (neat)	–	–	53	–	180	148	420	36 ± 1.0	223 ± 85	1170 ± 37
10 wt% PLimC	9.8 ± 5.1/0.39 ± 0.29	3.5 ± 3.8/0.7 ± 1.0	53	–	179	155	n.d.	32 ± 2.0	11 ± 1.7	1143 ± 50
30 wt% PLimC	39 ± 23/4.3 ± 3.8	7.1 ± 7.2/2.3 ± 2.4	53	–	179	154	250/420	19 ± 4.0	1.5 ± 0.3	1580 ± 109

[a] SEM (top values): Average area (µm²) was calculated from minimum 100 domains (Table S2); Raman (bottom values): Average area (µm²) was calculated from minimum 60 domains (PA12 blends ≈30 domains) (Table S2). The given diameters correspond to the area of an equivalent circle. For bimodal distributions only the average values for smaller droplets are given, values for larger droplets are presented in Table S2; [b] DSC: Glass transition temperature (T_g), cold crystallization temperature (T_{cc}), meltingtemperature (T_m) and crys-tallization temperature (T_c) were determined from the 2nd heating or cooling traces (scanningrate 10 K min^{-1} under nitrogen) except for PA12, where the 1st heating trace was used. TGA: Temperature at 5% weight loss ($T_{5\%}$) was determined by TGA measurements at 10 K min^{-1} under nitrogen. The first value refers to PLimC, whereas the second value refers to the matrixpolymer; [c] A test speed of 0.5 mm min^{-1} was used to determine the tensile strength (σ_m), elongation at break (%) and E-modulus of all blends besides PBAT. A test speed of 40 mm min^{-1} (PBAT) was used to determine σ_m and ϵ_{br}, respectively. Given values correspond to the average of 3 measurements.

PLA/poly(ϵ-caprolactone) blends.[36] TGA shows a distinct two-step degradation, with temperatures at 5% mass loss of $T_{5\%} = 250$ °C for PLimC and $T_{5\%} = 335$ °C for PLA, respectively (Figure 2C). Mass loss at each stage correlates with the weight percentages of the respective polymers in the blend. In PLA/PLimC blends $T_{5\%}$ for PLimC is significantly higher than in neat PLimC ($T_{5\%} = 230$ °C), whereas the $T_{5\%}$ of the PLA matrix is hardly influenced (Table 2). Here, the assumption is that the PLA matrix protects the encapsulated PLimC, resulting in an increased thermal stability of the dispersed PLimC phase. The E-modulus of heterogeneous blends with a dispersed droplet morphology can be estimated by the well-established series model ($E^{-1} = \Phi_1/E_1 + \Phi_2/E_2$, Φ_i = volume fraction of blend components), which describes the lower limit of the modulus, and the parallel model ($E = \Phi_1 E_1 + \Phi_2 E_2$), describing the upper limit, respectively.[37] Representative stress–strain curves for neat PLA and PLA/PLimC blends are shown in **Figure 3**A. The results from tensile testing show that the E-moduli are more predictable using the parallel model than the series model, but still higher than the parallel model would suggest (Figure 3B and Table 2). Tensile strength ($\sigma_m = 36 \pm 1$ MPa) and elongation at break ($\epsilon_{br} = 2.7 \pm 0.2\%$) were slightly decreased by the addition of PLimC, but still acceptable in comparison to neat PLA.

A possible reason for the comparably high E-moduli of the blends could be transesterification, which occurred during the blending process and increased the adhesion between PLimC and PLA. Gel permeation chromatography (GPC) of the produced blends showed on the one hand a significant broadening with a shift of the molar mass distribution toward both smaller and higher molar masses (especially in the blend with 30 wt% PLimC) in comparison to the GPCs of the pure blend components (Figure S7, Supporting Information). This indicates transesterification reactions and, thus, the formation of block-type copolymer structures during melt processing. Similar results were found by Wacharawichanant et al., who investigated PLA/poly(ethylene-co-methyl acrylate) (EMAC)/clay blends.[38] The E-modulus of PLA/EMAC blends increased significantly by the addition of clay, whereas tensile strength was slightly decreased. An increased adhesion between PLA and EMAC due to the clay was suggested as an explanation.

2.3. Blends with PBAT

The produced PBAT/PLimC blends show opaque strands after processing, which points again to phase-separated, immiscible blends (Figure S8, Supporting Information), which is confirmed by morphological studies. SEM and Raman imaging show the presence of dispersed PLimC droplets with a bimodal size distribution, consisting of small PLimC droplets in the µm-range and
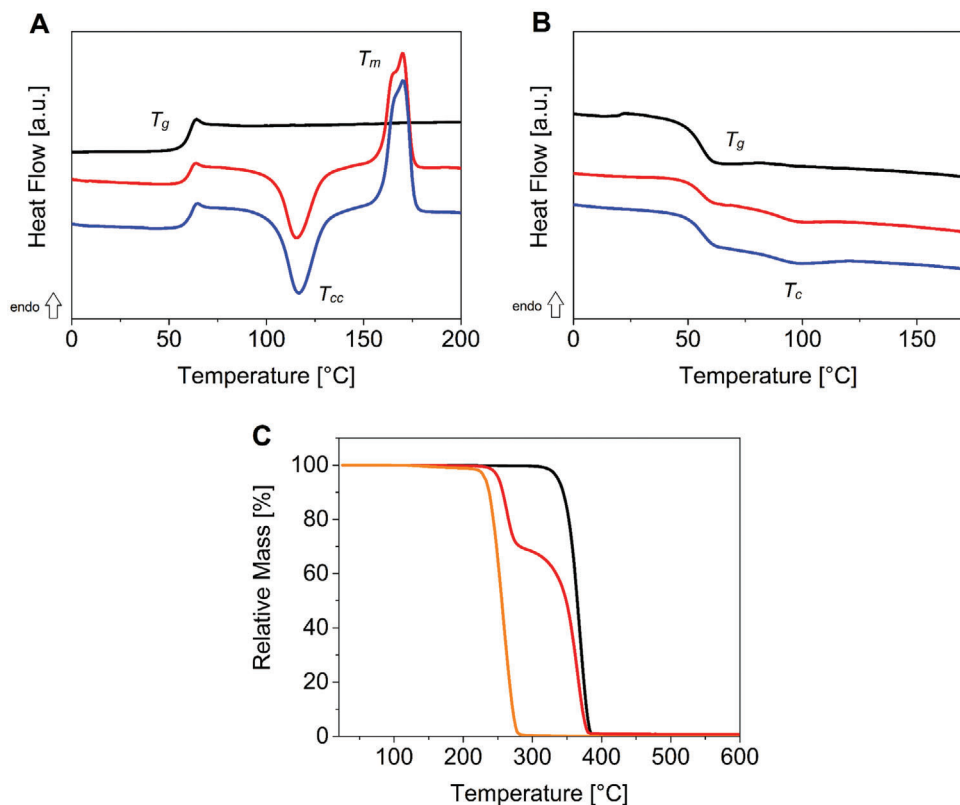
Figure 2. A) DSC second heating and B) cooling traces of PLA/PLimC blends (scanning rate 10 K min^{-1}). C) TGA of PLA/PLimC blends. PLA/PLimC = 100/0 w/w (black); PLA/PLimC = 90/10 w/w (red); PLA/PLimC = 70/30 w/w (blue); PLA/PLimC = 0/100 w/w (orange).

significantly larger PLimC domains with diameters of $D > 10$ µm (**Figure 4** and Figure S10, Supporting Information). The respective histograms for PLimC droplet size distributions are given in Figure S9, Supporting Information. For the smaller PLimC droplets average diameters of $D = 1.6 \pm 1.7$ µm (from SEM) and $D = 1.3 \pm 1.9$ µm (from Raman imaging) were determined for the PBAT/PLimC = 90/10 w/w blend, and $D = 1.1 \pm 1.8$ µm (from SEM) and $D = 0.9 \pm 1.8$ µm (from Raman imaging) for the PBAT/PLimC = 70/30 w/w blend, respectively (Table 2). The bimodal size distribution of PLimC droplets can be explained by the

high melt viscosity contrast between both polymers (PLimC: η_0 = 890 kPa·s,[25] PBAT: η_0 = 2.7 kPa·s[29]) in combination with the significantly stronger incompatibility (difference in solubility parameters; PBAT: δ = 22.3 MPa$^{1/2}$,[28] PLimC: δ = 17.6 MPa$^{1/2}$[14]) between PBAT/PLimC with respect to PLA/PLimC (Table 1). Consequently, the shear forces during compounding are not high enough to break up the PLimC droplets effectively, resulting in the observed bimodal size distribution.

The observed phase separation is also reflected in the thermal properties of the blends (**Figure 5**A,B and Table 2), showing a
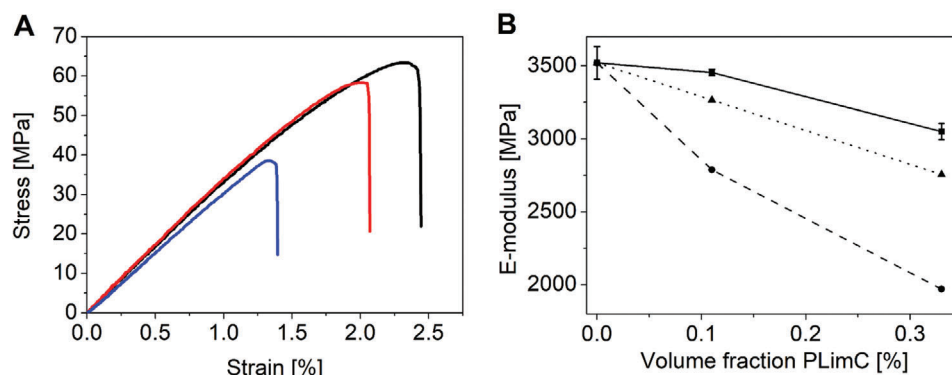
Figure 3. A) Representative stress–strain curves for neat PLA (black) and PLA/PLimC blends (PLA/PLimC = 90/10 w/w (red), PLA/PLimC = 70/30 w/w (blue). B) E-moduli of PLA/PLimC blends (solid) in dependence of the volume fraction of PLimC and estimated E-moduli of the blends employing the series (dashed) and parallel (dotted) model, respectively.
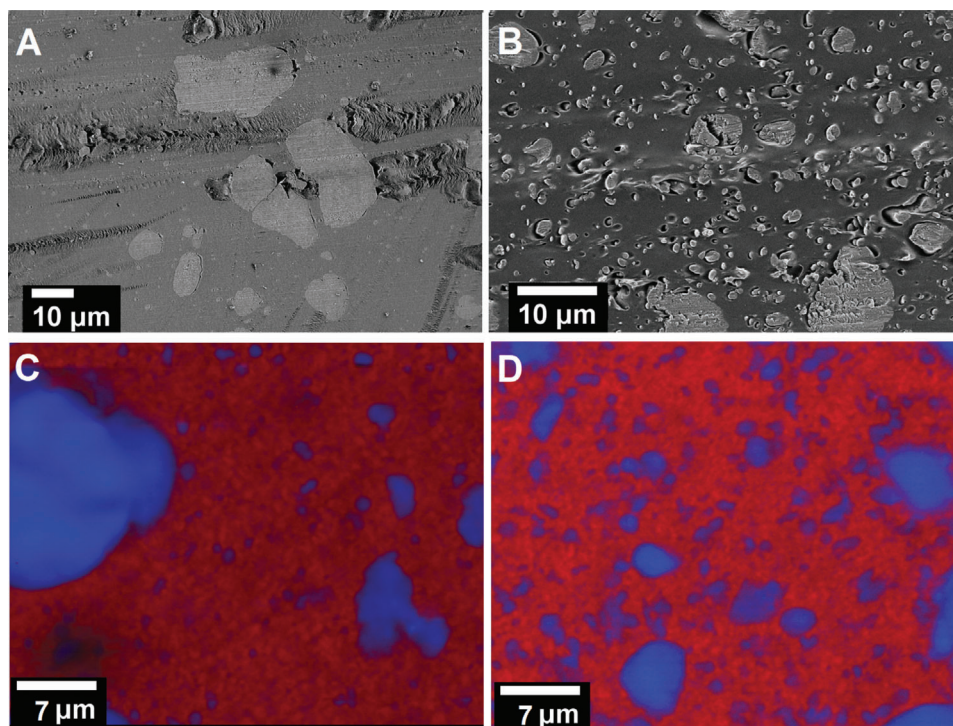
Figure 4. SEM (PLimC appears bright) and Raman imaging (PLimC domains are colored in blue) of PBAT/PLimC blends: A,C) PBAT/PLimC = 90/10 w/w, B,D) PBAT/PLimC = 70/30 w/w. The corresponding Raman spectra of each component are given in Figure S4, Supporting Information.
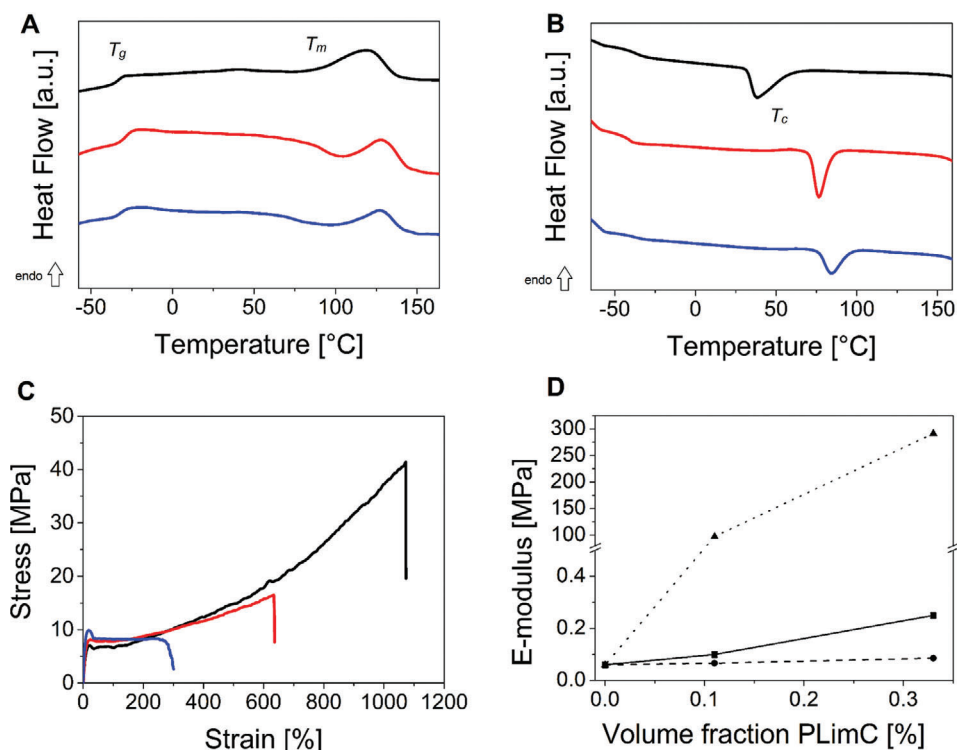
Figure 5. A) DSC second heating and B) cooling traces (scanning rate 10 K min^{-1}), and C) representative stress–strain curves for neat PBAT (black) and PBAT/PLimC blends (PBAT/PLimC = 90/10 w/w (red), PBAT/PLimC = 70/30 w/w (blue)). D) E-moduli of PBAT/PLimC blends (solid) in dependence of the volume fraction of PLimC. Estimated E-moduli of the blends employing the series (dashed) and parallel (dotted) model, respectively.
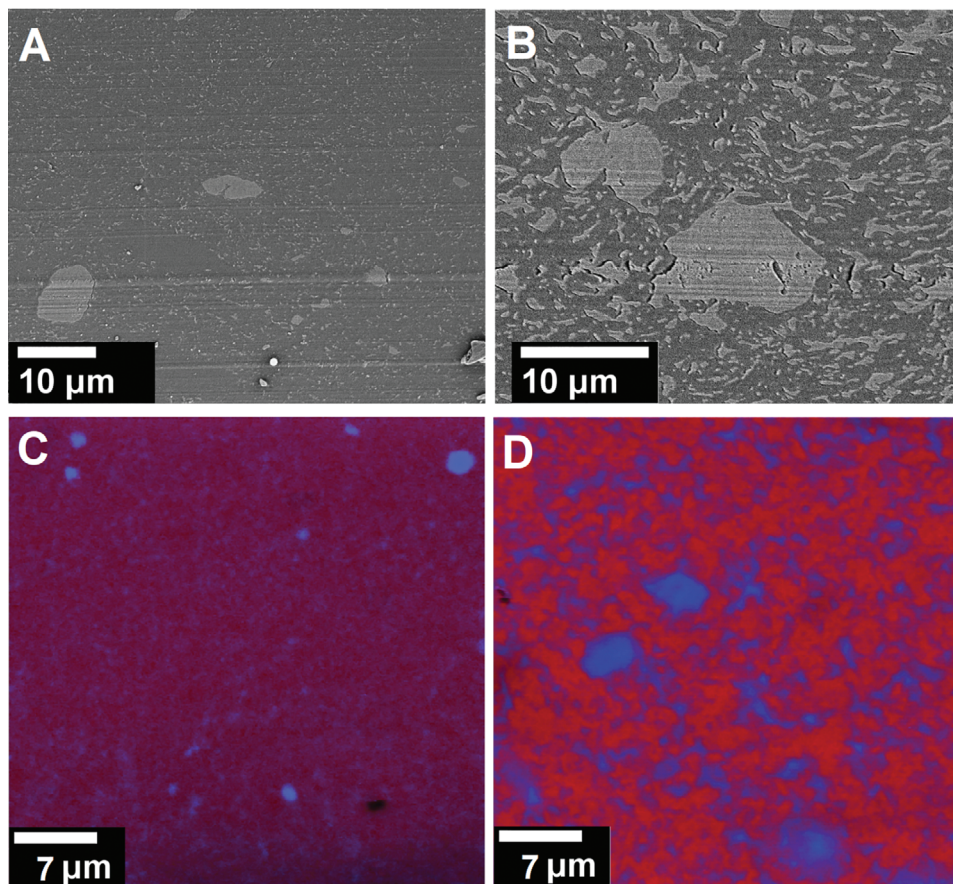
Figure 6. SEM (PLimC appears bright) and Raman imaging (PLimC domains are colored in blue) of COPE/PLimC blends: A,C) COPE/PLimC = 90/10 w/w, B,D) COPE/PLimC = 70/30 w/w. The corresponding Raman spectra of each component are given in Figure S4, Supporting Information.

glass transition temperature for the PBAT matrix of $T_g = -28\,°C$, being almost identical to that of neat PBAT ($T_g = -30\,°C$). The T_g of pure PLimC is $128\,°C$ (Figure S6, Supporting Information) and is hidden underneath the melting transition of PBAT. The crystallization temperature of neat PBAT ($T_c = 42\,°C$) is increased significantly in PBAT/PLimC blends ($\approx T_c = 84\,°C$). The same behavior was observed for PLA/PLimC blends and might be attributed to a nucleating effect of the interface between PLimC and the matrix polymer. TGA also reveals an increased stability of PLimC ($T_{5\%} = 253\,°C$) in the PBAT matrix, like it was observed for PLA/PLimC blends (Figure S11, Supporting Information).

Focusing on the mechanical properties of PBAT/PLimC blends, the influence of PLimC on the E-modulus is most pronounced (Figure 5C,D and Table 2). Blending PBAT with 30 wt% PLimC increases the E-modulus about three times from $E = 92 \pm 19$ MPa for neat PBAT to $E = 247 \pm 12$ MPa for the blend. At the same time, elongation at break is decreased, but still shows reasonably high values of $\epsilon_{br} \approx 200\%$. This combination of an increased E-modulus with high elongation at break makes PBAT/PLimC blends interesting for applications, despite their inhomogeneous blend morphology with a bimodal PLimC droplet distribution. In general, the E-moduli of the blends are close to the prediction from the series model (Figure 5D). This is reasonable, because the E-modulus of the PBAT matrix is sub-stantially lower compared to that of the dispersed PLimC phase and due to the incompatibility of the blend partners the interfacial interactions are expected to be rather weak.

2.4. Blends with Arnitel EM400

Arnitel EM400 is a COPE with poly(butylene terephthalate) (PBT) hard segments and polytetrahydrofuran (PTHF) soft segments (PBT/PTHF = 40/60 w/w), which shows similarities in structure to PBAT and of all investigated polymers its solubility parameter is closest to that of PLimC (Table 1). SEM and Raman imaging clearly show that the produced COPE/PLimC blends (optical photographs in Figure S12, Supporting Information) are phase-separated with a bimodal distribution of PLimC domains dispersed in the COPE matrix, that is, similar to the morphology observed for the PBAT/PLimC blends. This is quite reasonable, because COPE and PBAT have similarities in structure. The small PLimC domains are finely distributed over the whole COPE matrix, showing average diameters of $D = 0.4 \pm 1.3$ µm (COPE/PLimC = 90/10 w/w) and $D = 1.5 \pm 1.7$ µm (COPE/PLimC = 70/30 w/w) as determined by SEM (**Figure 6** and Figures S13 and S14, Supporting Information). It is noted that PLimC droplet size of the COPE blend with 10 wt% PLimC

**ADVANCED
SCIENCE NEWS**

www.advancedsciencenews.com

**Macromolecular
Materials and Engineering**

www.mame-journal.de
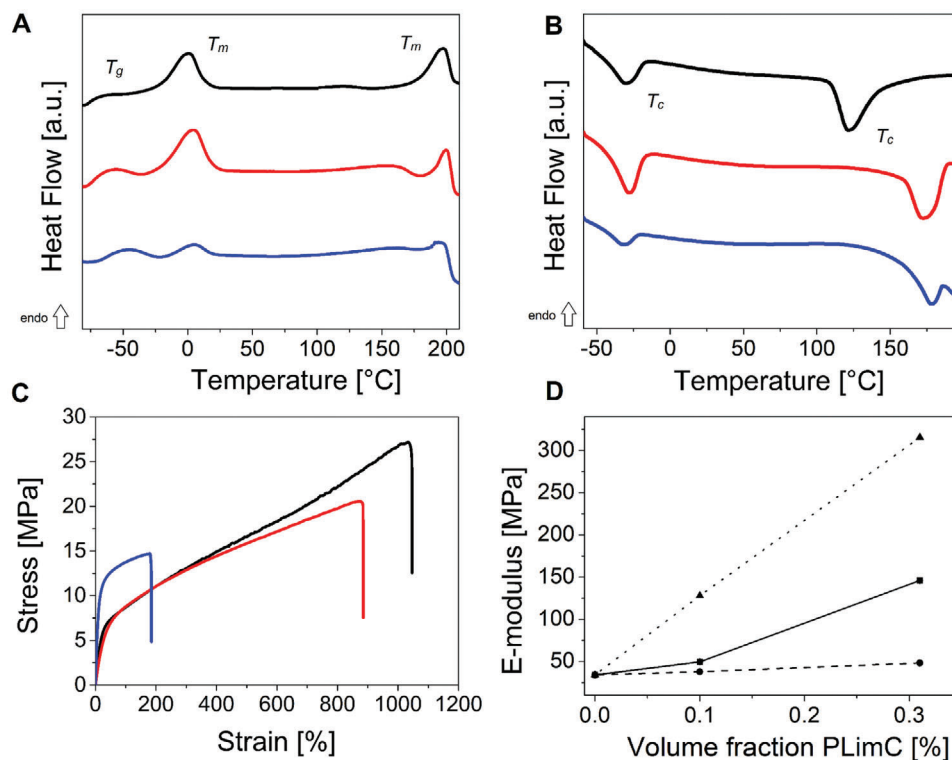
Figure 7. A) DSC second heating and B) cooling traces of COPE/PLimC blends (scanning rate 10 K min^{-1}). C) Representative stress–strain curves for neat COPE (black) and COPE/PLimC blends (COPE/PLimC = 90/10 w/w (red); COPE/PLimC = 70/30 w/w (blue). D) E-moduli of COPE/PLimC blends (solid) in dependence of the volume fraction of PLimC. Estimated E-moduli of the blends employing the series (dashed) and parallel (dotted) model, respectively.

is smaller compared to that of the respective PBAT/PLimC blend, which might be attributed to the higher compatibility (smaller difference in solubility parameters). Raman imaging confirms the measured values with an average size of $D = 0.6 \pm 1.8$ μm (COPE/PLimC = 90/10 w/w) and $D = 0.8 \pm 1.9$ μm (COPE/PLimC = 70/30 w/w). The larger PLimC domains show sizes of $D \approx 10$ μm, being slightly lower compared to that in PBAT/PLimC blends. Despite the better compatibility of COPE and PLimC a bimodal size distribution can be found. This is due to the greater viscosity contrast between PLimC and COPE (Table 1).

The investigation of thermal properties of neat COPE and COPE/PLimC blends revealed similar glass transition temperatures for the PTHF soft segment ($T_g \approx -70$ °C) (**Figure 7**A). The influence of PLimC on T_c and T_m of the PTHF soft segment was negligible, whereas T_c of the PBT hard segment ($T_c \approx 175$ °C) was significantly increased in comparison to neat COPE ($T_c \approx 122$ °C) (Figure 7B and Table 2). This might again be attributed to a nucleation effect of the COPE/PLimC domain interface. In line with the TGA results of the above discussed blends PLimC showed an increased temperature stability ($T_{5\%} = 253$ °C) in COPE/PLimC blends (Figure S15, Supporting Information).

Due to similarities in structure of PBAT and COPE and the respective blend morphologies comparable mechanical properties were observed (Figure 7C,D and Table 2). The E-modulus showed a fourfold increase from $E = 34 \pm 5.8$ MPa for neat COPE to $E = 146 \pm 11$ MPa for the COPE/PLimC = 70/30

w/w blend, while the elongation at break decreased but still stayed in an acceptable range for applications ($\epsilon_{br} \approx 200\%$). The E-moduli of the blends are closer to the values predicted from the series model rather than the parallel model, in analogy to PBAT/PLimC blends (Figure 5D). This might be ascribed to the rather high difference in E-modulus of both homopolymers (Table 2) and a weak interfacial adhesion between the blend partners.

2.5. Blends with PA12

The last explored blend partner, the aliphatic polyamide PA12, shows a fundamentally different chemical structure than the above investigated polyesters, so different results for PA12/PLimC blends might be expected (optical photographs of the produced blends are displayed in Figure S16). Morphology investigations with SEM and Raman imaging revealed a bimodal size distribution also for this type of blend system (**Figure 8** and Figures S17 and S18, Supporting Information). However, the average PLimC domain sizes were significantly higher compared to that of the other blend systems studied (Table 2 and Figure S2, Supporting Information). For PA12 blends with 10 wt% PLimC average PLimC droplet sizes of $D = 3.5 \pm 3.8$ μm and $D = 11 \pm 11$ μm were obtained from SEM image evaluation, and $D = 7.1 \pm 7.2$ μm and $D = 20 \pm 20$ μm for the blend with 30 wt% PLimC, respectively. Raman imaging, where mostly the small droplets

**ADVANCED
SCIENCE NEWS**

www.advancedsciencenews.com

**Macromolecular
Materials and Engineering**

www.mame-journal.de
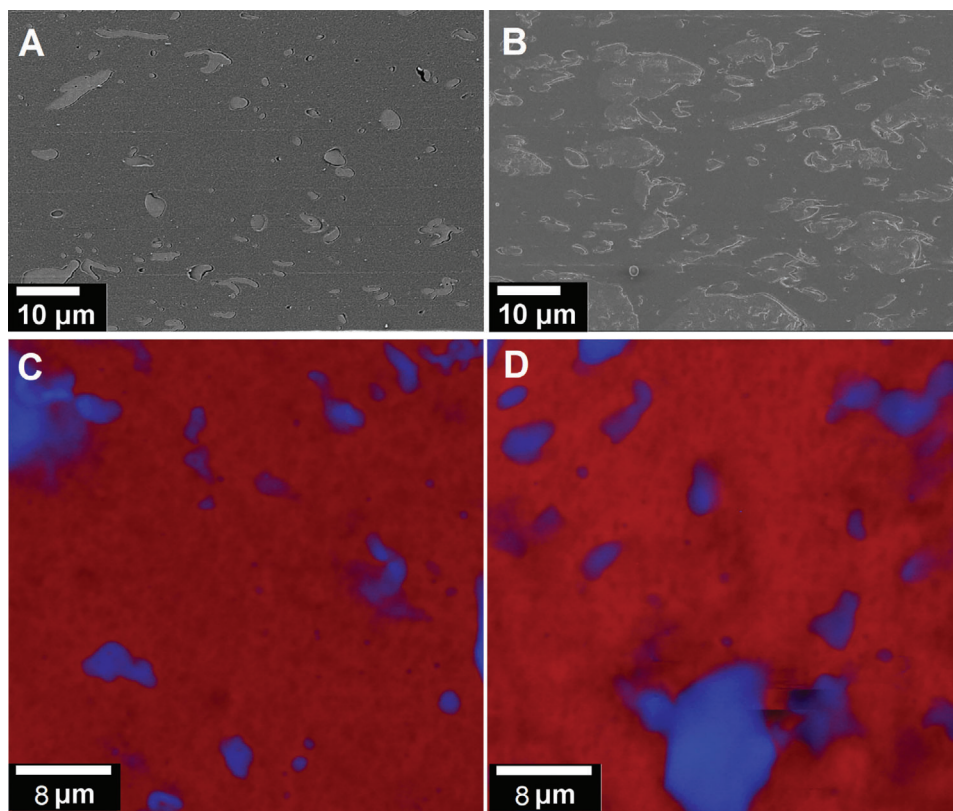
Figure 8. SEM (PLimC appears bright) and Raman imaging (PLimC domains are colored in blue) of PA12/PLimC blends. A,C) PA12/PLimC = 90/10 w/w, B,D) PA12/PLimC = 70/30 w/w. The corresponding Raman spectra of each component are given in Figure S4, Supporting Information.

were probed, that is, the lower size fraction of the bimodal distribution, showed PLimC droplets in the same order of magnitude ($D = 0.7 \pm 1.0$ µm for PA12/PLimC = 90/10 w/w and $D = 2.3 \pm 2.4$ µm for PA12/PLimC = 70/30 w/w). The comparably broad bimodal size distribution in PA12/PLimC blends most likely originates from the low melt viscosity of PA12 in combination with its rather high incompatibility (large difference in solubility parameters, Table 1) to PLimC. Consequently, the shear forces during processing might be not high enough to split the PLimC droplets further, resulting in larger PLimC domains. The strongly phase-separated structure of the blends is also manifested in the thermal properties, revealing similar glass transition temperatures for PA12 in the PA12/PLimC blends with respect to neat PA12 ($T_g \approx 53$ °C, Table 2). It is noted that in this case glass transition temperatures could only be detected in the first heating run (Figure S19A, Supporting Information). The crystallization temperature is only slightly increased by 7 °C from $T_c = 148$ °C for neat PA12 to $T_c = 155$ °C for the PA12/PLimC blend with 30 wt% PLimC, whereby the PA12 melting temperature is hardly influenced (**Figure** 9A,B). This indicates that the nucleation effect of the PLimC domains, respective the PA12/PLimC interface, is not as strong as in PLA, PBAT, or COPE blends. TGA analysis also shows the stabilizing effect of the polymer matrix on PLimC with an observed increase in $T_{5\%}$ (PLimC) by ≈ 20 °C (Figure S19B, Supporting Information).

As the E-moduli of both blend components (PA12 and PLimC) are quite similar (≈ 1000 MPa), no significant effect

of composition on the E-modulus of the blends is expected and also predicted by both the series and parallel model (Figure S19C, Supporting Information). The observed deviation in the E-modulus of the PA12/PLimC = 70/30 w/w blend, which showed a much higher value than predicted, can be attributed to the very inhomogeneous blend morphology giving rise to a very high standard deviation for this blend composition. The stress–strain traces presented in Figure 9C clearly show that the addition of PLimC has a detrimental effect on the elongation at break, which was drastically reduced down to $\epsilon_{br} \approx 2\%$ for the PA12/PLimC = 70/30 w/w blend. This in turn makes this blend system rather unattractive for applications.

3. Conclusion

In this paper, blends of various commodity polymers with PLimC as minority component (10–30 wt%) were investigated. Blends with PS and PMMA (similar glass transition temperature to PLimC) were very brittle and blends with PA12 showed very low elongation at break. The most promising results were obtained for blends with polymers exhibiting a similar chemical structure to PLimC, that is, PLA, PBAT, and COPE (aliphatic/aromatic polyester). The most homogeneous morphology was observed for PLA/PLimC blends, probably due to transesterification and formation of PLA/PLimC block-type structures during processing (acting as compatibilizers). In terms of mechanical properties

**ADVANCED
SCIENCE NEWS**

www.advancedsciencenews.com

**Macromolecular
Materials and Engineering**

www.mame-journal.de
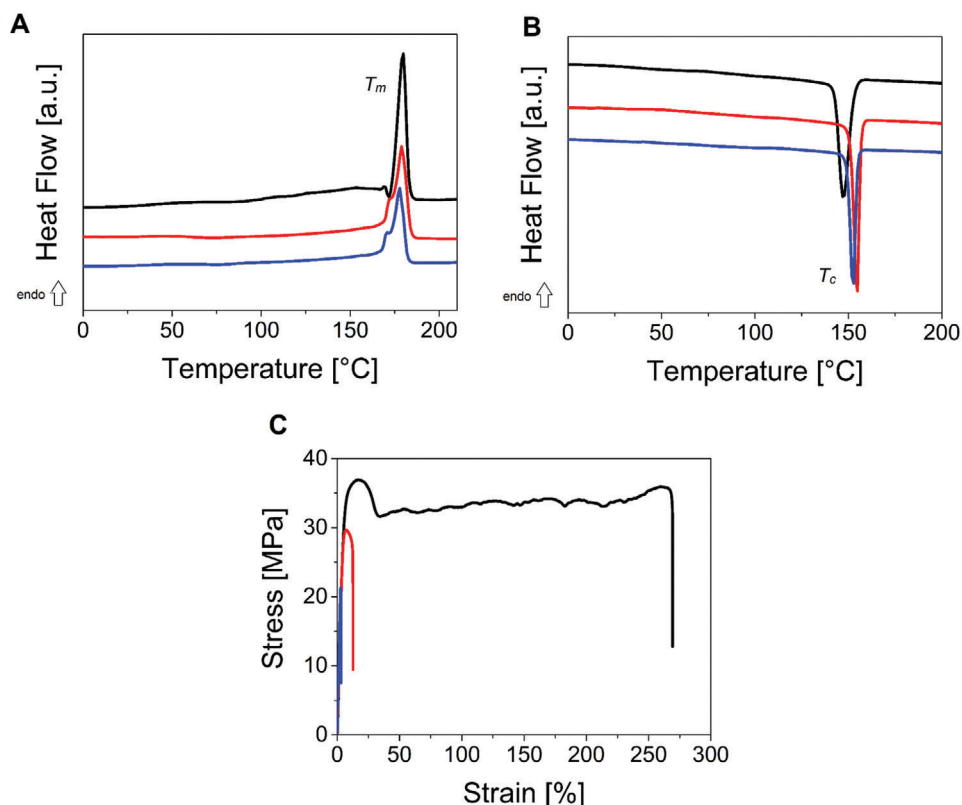
Figure 9. A) DSC second heating and B) cooling traces of PA12/PLimC blends (scanning rate 10 K min^{-1}). C) Representative stress–strain curves for neat PA12 (black) and PA12/PLimC blends (PA12/PLimC = 90/10 w/w (red); PA12PLimC = 70/30 w/w (blue).

PBAT and COPE blends were the most promising, as they combine a comparably high E-modulus (to pure PBAT and COPE) with reasonably high elongations at break up to 200%. These results show the potential of PLimC for the production of more sustainable polymer blends via blending with petrol- or food-based polymers, having similar chemical structures compared to PLimC. For the other polymers the use of compatibilizers like block copolymers could improve the phase connectivity. Besides, the observed increased thermal stability of PLimC in the investigated blends together with the nucleation effect of the matrix/PLimC interface for semicrystalline matrix polymers (increase in crystallization temperature) can add additional benefits to PLimC blends, resulting for example in lower cycle times for PLA/PLimC blends due to improved PLA crystallization.

4. Experimental Section

Materials and Blend Processing: The used PLimC (M_n = 65 kDa, Đ = 1.09) was synthesized according to literature procedures.[6] In general, the blends were produced as follows. Polymers were pre-dried at 0.1 mbar and 80 °C for 16 h. In a double screw compounder (DSM Micro 15cc Twin Screw Compounder, Company: Xplore) 8–14 g polymer were processed to form binary blends. Blending was performed at 50 rpm for 4 min. PLimC was used as minority blend component with contents of 10 and 30 wt%. The neat blending partners (matrix polymers) were also processed as a reference. Specifications of the employed matrix polymers and the processing parameters, like rotational speed or processing time can be found

in Table 1. The solubility parameter of Arnitel EM400 was calculated from the composition of the COPE: PBT/PTHF 40/60 w/w (PBT 22.7,[30] PTHF 16.8[30]).

Methods: SEM images were taken with a Zeiss LEO 1530 (FE-SEM with Schottky-field-emission cathode and In-lens detector) using an accelerating voltage of 3–10 kV. Small fragments of the samples were mounted on a standard sample holder by conductive adhesion graphite-pad (Plano) for SEM examination. For cyro-microtomy of polymer blends a Leica EM VC7 microtome was used. The ultrathin sections were treated with OsO$_4$ vapor overnight in order to selectively stain the PLimC domains (appear bright in the SEM micrographs). SEM was performed on microtome cuts and as well on the surface of small sample fragments.

The average domain sizes were determined by measuring at least 100 (SEM) and 30 (Raman imaging) particles using ImageJ software (1.52a).[35] Detailed overview over all analyzed particles can be found in the supporting information. For the calculation of the particle diameters, the area of each PLimC domain was measured using the ImageJ software. Then, assuming that droplets are fully spherical particles and the cuts have gone through the middle of each droplet, the diameter corresponding to the area was back calculated. Of course, these assumptions cannot be 100% fulfilled, hence resulting in the relatively large standard deviations.

DSC was performed on a Netzsch 204 F1 Phoenix using a scanning rate of 10 K min^{-1} under N$_2$ atmosphere. Glass transition temperature (T_g), cold crystallization temperature (T_{cc}), melting temperature (T_m), and crystallization temperature (T_c) were determined from the 2nd heating or cooling traces (scanning rate 10 K·min^{-1} under nitrogen) except for PA12, where the 1st heating trace was used.

TGA was conducted on a Netzsch TG 209 F1 Libra at a scanning rate of 10 K min^{-1} under N$_2$ atmosphere. Temperature at 5% weight loss ($T_{5\%}$) was determined by TGA measurements at 10 K min^{-1} under nitrogen. In

Table 2, the first value refers to PLimC, whereas the second value refers to the matrix polymer.

For CHCl$_3$-GPC analyses an Agilent 1200 system equipped with a SDV precolumn (particle size 5 µm; PSS Mainz), a SDV linear XL column (particle size 5 µm, PSS Mainz), and a refractive index (RI) detector (Agilent Technologies 1260 Infinity) was used. Toluene (HPLC grade) was used as internal standard and CHCl$_3$ (HPLC grade) was used as solvent at a flow rate of 0.5 mL min^{-1} at room temperature. Calibration was based on narrowly distributed PS standards.

HFIP-GPC was conducted with an Agilent 1200 system equipped with a SDV precolumn (particle size 7 µm; PSS Mainz), a SDV linear XL column (particle size 7 µm, PSS Mainz) and a RI detector (Gynotek SE-61, Agilent Technologies). Toluene (HPLC grade) was used as internal standard. Calibration was done with narrowly distributed PMMA standards from the company PSS Mainz. HFIP with potassium trifluoroacetate ($c = 8$ g L^{-1}) was used as solvent at a flow rate of 0.5 mL min^{-1} at room temperature.

For Raman imaging a WITec alpha 300 RA+ imaging system equipped with an UHTS 300 spectrometer and a back-illuminated Andor Newton 970 EMCCD (electron multiplying charge-coupled device) camera was employed. The measurements were conducted with an excitation wavelength of $\lambda = 352$ nm and a typical integration time of 0.35 s pixel^{-1} using a laser power of 10 mW (100× objective, NA = 0.9, step size 100 nm pixel^{-1}). All spectra were subjected to a cosmic ray removal routine and baseline correction using WITec project 5.2. The spatial distribution of the components was extracted from the Raman imaging data employing the Raman spectra of the neat components (Figure S4, Supporting Information), employing the True Component Analysis in WITec project 5.2.

Samples for mechanical testing were prepared from extruded polymer strands, which were filled in a metal frame (13 cm × 13 cm) with a thickness of 1.0 mm and hot-pressed for 5 min by applying a force of 10 kN. After obtaining the hot-pressed polymer plates, dogbone-shaped specimens were punched for tensile testing according to DIN53504S3A, employing a Coesfeld Material punching machine (model 951617).

A Zwick/Roell Z0.5 tensile tester was used for tensile testing. The preload for all blends was 0.02 MPa. A test speed of 0.5 mm min^{-1} was used to determine the tensile strength (σ_m), elongation at break (ϵ_{br}), and E-modulus of all blends besides PBAT. For PBAT a test speed of 40 mm min^{-1} was employed to determine tensile strength and elongation at break, respectively. Given values correspond to the average of 3 measurements.

Supporting Information

Supporting Information is available from the Wiley Online Library or from the author.

Conflict of Interest

The authors declare no conflict of interest.

Data Availability Statement

Data sharing is not applicable to this article as no new data were created or analyzed in this study.

[1] a) Y. Zhu, C. Romain, C. Williams, *Nature* **2016**, *540*, 354; b) H. Nakajima, P. Dijkstra, K. Loos, *Polymers* **2017**, *9*, 523; c) D. Schneiderman, M. A. Hillmyer, *Macromolecules* **2017**, *50*, 3733; d) X. Zhang, M. Fevre, G. O. Jones, R. M. Waymouth, *Chem. Rev.* **2018**, *118*, 839; e) G.-Q. Chen, M. K. Patel, *Chem. Rev.* **2012**, *112*, 2082; f) S. Spierling, E. Knüpffer, H. Behnsen, M. Mudersbach, H. Krieg, S. Springer, S. Albrecht, C. Herrmann, H.-J. Endres, *J. Cleaner Prod.* **2018**, *185*, 476.

[2] S. A. Attaran, A. Hassan, M. U. Wahit, *J. Thermoplast. Compos. Mater.* **2017**, *30*, 143.

[3] a) D. J. Darensbourg, *Chem. Rev.* **2007**, *107*, 2388; b) A. J. Kamphuis, F. Picchioni, P. P. Pescarmona, *Green Chem.* **2019**, *21*, 406; c) M. Scharfenberg, J. Hilf, H. Frey, *Adv. Funct. Mater.* **2018**, *18*, 760.

[4] S. J. Poland, D. J. Darensbourg, *Green Chem.* **2017**, *19*, 4990.

[5] A. Wambach, S. Agarwal, A. Greiner, *Sustainable Chem. Eng.* **2020**, *8*, 14690.

[6] O. Hauenstein, M. Reiter, S. Agarwal, B. Rieger, A. Greiner, *Green Chem.* **2016**, *18*, 760.

[7] M. Winkler, C. Romain, M. A. R. Meier, C. K. Williams, *Green Chem.* **2015**, *17*, 300.

[8] C. M. Byrne, S. D. Allen, E. B. Lobkovsky, G. W. Coates, *J. Am. Chem. Soc.* **2004**, *126*, 11404.

[9] C. Martín, A. Kleij, *Macromolecules* **2016**, *49*, 6285.

[10] L. Peña Carrodeguas, J. González-Fabra, F. Castro-Gómez, C. Bo, A. W. Kleij, *Chemistry* **2015**, *21*, 6115.

[11] a) N. Kindermann, À. Cristòfol, A. W. Kleij, *ACS Catal.* **2017**, *7*, 3860; b) F. Auriemma, C. de Rosa, M. R. Di Caprio, R. Di Girolamo, W. C. Ellis, G. W. Coates, *Angew. Chem. Int. Ed.* **2015**, *54*, 1215; c) C. Li, R. J. Sablong, C. Koning, *Angew. Chem. Int. Ed.* **2016**, *55*, 11572; d) C. Li, R. J. Sablong, C. Koning, *Eur. Polym. J.* **2015**, *67*, 449.

[12] O. Hauenstein, M.d. M. Rahman, M. Elsayed, R. Krause-Rehberg, S. Agarwal, V. Abetz, A. Greiner, *Adv. Mater. Technol.* **2017**, *2*, 1700026.

[13] a) O. Hauenstein, S. Agarwal, A. Greiner, *Nat. Commun.* **2016**, *7*, 11862; b) T. Stößer, C. Li, J. Unruangsri, P. K. Saini, R. J. Sablong, M. A. R. Meier, C. K. Williams, C. Koning, *Polym. Chem.* **2017**, *8*, 6099; c) C. Li, R. J. Sablong, R. A. T. M. van Benthem, C. E. Koning, *ACS Macro Lett.* **2017**, *66*, 684.

[14] J. Bailer, S. Feth, F. Bretschneider, S. Rosenfeldt, M. Drechsler, V. Abetz, H. Schmalz, A. Greiner, *Green Chem.* **2019**, *21*, 1495.

[15] F. Parrino, A. Fidalgo, L. Palmisano, L. M. Ilharco, M. Pagliaro, R. Ciriminna, *ACS Omega* **2018**, *3*, 4884.

[16] D. Zhang, E. A. del Rio-Chanona, J. L. Wagner, N. Shah, *Sustainable Prod. Consumption* **2018**, *14*, 152.

[17] M. Sheth, R. A. Kumar, V. Dav, R. A. Gross, S. P. McCarthy, *J. Appl. Polym. Sci.* **1997**, *66*, 1495.

[18] A. M. Gajria, V. Davé, R. A. Gross, S. P. McCarthy, *Polymer* **1996**, *37*, 437.

[19] Y. F. Kim, C. N. Choi, Y. D. Kim, K. Y. Lee, M. S. Lee, *Fibers Polym.* **2004**, *5*, 270.

[20] G. Biresaw, C. J. Carriere, *J. Polym. Sci., Part B: Polym. Phys.* **2002**, *40*, 2248.

[21] M. Evstatiev, S. Simeonova, K. Friedrich, X.-Q. Pei, P. Formanek, *J. Mater. Sci.* **2013**, *48*, 6312.

[22] a) M. Larsson, O. Markbo, P. Jannasch, *RSC Adv.* **2016**, *6*, 44354; b) Y. Ke, X. Y. Zhang, S. Ramakrishna, L. M. He, G. Wu, *Mater. Sci. Eng. C*

ADVANCED
SCIENCE NEWS

www.advancedsciencenews.com

Macromolecular
Materials and Engineering

www.mame-journal.de

2017, *70*, 1107; c) E. Renard, M. Walls, P. Guérin, V. Langlois, *Polym. Degrad. Stab.* **2004**, *85*, 779.

[23] a) M. Harada, T. Ohya, K. Iida, H. Hayashi, K. Hirano, H. Fukuda, *J. Appl. Polym. Sci.* **2007**, *49*, 1215; b) M. Shibata, Y. Inoue, M. Miyoshi, *Polymer* **2006**, *82*, 1028; c) Z. Qiu, T. Ikehara, T. Nishi, *Polymer* **2003**, *22*, 395.

[24] a) B. Imre, B. Pukánszky, *Eur. Polym. J.* **2013**, *49*, 1215; b) K. M. Zia, A. Noreen, M. Zuber, S. Tabasum, M. Mujahid, *Int. J. Biol. Macromol.* **2016**, *82*, 1028; c) J. J. Koh, X. Zhang, C. He, *Int. J. Biol. Macromol.* **2018**, *109*, 99.

[25] S. Neumann, L.-C. Leitner, H. Schmalz, S. Agarwal, A. Greiner, *Sustainable Chem. Eng.* **2020**, *8*, 6442.

[26] E. Meaurio, E. Sanchez-Rexach, E. Zuza, A. Lejardi, A. d. P. Sanchez-Camargo, J.-R. Sarasua, *Polymer* **2017**, *113*, 295.

[27] T. Standau, H. Long, S. Murillo Castellón, C. Brütting, C. Bonten, V. Altstädt, *Materials* **2020**, *13*, 1371.

[28] R. Muthuraj, M. Misra, A. K. Mohanty, *J. Polym. Environ.* **2014**, *22*, 336.

[29] D. Kanev, E. Takacs, J. Vlachopoulos, *Int. Polym. Process.* **2007**, *22*, 395.

[30] C. Wohlfarth, M. D. Lechner, K. F. Arndt, *Polymer Solutions: Physical Properties and their Relations I (Thermodynamic Properties: pVT-Data and Miscellaneous Properties of Polymer Solutions)*, Springer, New York **2010**.

[31] H. Veenstra, B. Norder, J. van Dam, A. Posthuma de Boer, *Polymer* **1999**, *40*, 5223.

[32] B. Haworth, N. Hopkinson, D. Hitt, X. Zhong, *Rapid Prototyping J.* **2013**, *19*, 28.

[33] J. E. Mark, *Polymer Data Book*, Oxford University Press, New York **1990**.

[34] C. J. Carriere, A. Cohen, *J. Rheol.* **1991**, *35*, 205.

[35] W. S. Rasband, *ImageJ*, U. S. National Institutes of Health, Bethesda, MD **1997**–2018.

[36] M. Rizzuto, L. Marinetti, D. Caretti, A. Mugica, M. Zubitur, A. J. Müller, *CrystEngComm* **2017**, *19*, 3178.

[37] H. Ruckdäschel, J. K. W. Sandler, V. Altstädt, H. Schmalz, V. Abetz, A. H. E. Müller, *Polymer* **2007**, *48*, 2700.

[38] S. Wacharawichanant, S. Ratchawong, P. Hoysang, M. Phankokkruad, *MATEC Web Conf.* **2017**, *130*, 7006.